Metastable state of the photomagnetic Prussian blue analog K_{0.3}Co[Fe(CN)_{6}]_{0.77}·3.6H_{2}O investigated by various techniques

Christian Chong, Miho Itoi, Kamel Boukheddaden, Epiphane Codjovi, Aurelian Rotaru, François Varret, Franz A. Frye, Daniel R. Talham, Isabelle Maurin, Dmitry Chernyshov, and Miguel Castro

Phys. Rev. B **84**, 144102 — Published 4 October 2011

DOI: 10.1103/PhysRevB.84.144102

Unusual metastable state of the photo-magnetic Prussian blue analog $K_{0.3}Co[Fe(CN)_6]_{0.77} \cdot 4.4H_2O$, investigated by various physical techniques.

Christian Chong, Miho Itoi,* Kamel Boukheddaden,† Epiphane Codjovi, Aurelian Rotaru, and François Varret‡
Groupe d'Etudes de la Matière Condensée, UMR 8635,
CNRS-Université de Versailles Saint-Quentin-en-Yvelines,
45 Avenue des Etats Unis, 78035 Versailles, France

Franz A. Frye and Daniel R. Talham
Department of Chemistry, University of Florida, Gainesville, FL 32611-7200, USA

Isabelle Maurin
Laboratoire de Physique de la Matière Condensée,
UMR 7643, CNRS-Ecole Polytechnique,
Route de Saclay 91120 Palaiseau, France

Dmitry Chernyshov
Swiss-Norwegian Beam-Lines, European Synchrotron Radiation Facility, BP 220, 38048 Grenoble Cedex, France

Miguel Castro
Instituto de Ciencia de Materiales de Aragón, CSIC-Universidad de Zaragoza, Pedro Cerbuna 12, 50009 Zaragoza, Spain
(Dated: May 26, 2011)

The thermodynamic properties of the photomagnetic Prussian blue analog $K_{0.3}Co[Fe(CN)_6]_{0.77} \cdot 4.4H_2O$, which exhibits a charge-transfer induced spin transition (CTIST), are reported. According to the thermal history of the sample, different low-temperature states are obtained: a quenched high-spin state (Q), a low-spin state (LT) achieved through the decay of the Q state, and an "intermediate" state (IM) combining low-spin (LS) and high-spin (HS) local states. The IM state is obtained by slow cooling and displays a slight kinetic dependence. The long lifetime of the IM state, which persists up to the vicinity of the CTIST temperature, is unusual, and differs from all metastable states reported so far for photo-magnetic Prussian blue analogs. The properties of the different states and of their photo-excited counterparts are investigated by magnetic and photo-magnetic measurements, calorimetry, diffuse reflectance, and X-ray diffraction. A key feature of the IM state revealed by X-ray diffraction is the onset of phase separation between a LT-type fraction and a mixed HS-LS fraction (approx. 50 : 50). X-ray patterns of the IM state obtained during successive cooling and heating stages document irreversible transformations. The formation and properties of the IM state suggest a self-organization process between low-spin and high-spin sites in response to internal structural stresses, and this effect is hindered by irradiation with visible light. The relaxation kinetics of the Q and photo-excited states are analyzed by using a two-variable model which accounts for the onset of correlations due to short-range elastic interactions. A quantitative comparison to the analogous sodium compound, $Na_{0.32}Co[Fe(CN)_6]_{0.74} \cdot 3.4H_2O$, confirms the non-standard behavior of the title potassium compound and supports the structural origin of the self-organization processes.

PACS numbers: 75.50.Xx, 75.30.Wx, 64.60.My, 64.70.Kt
Keywords:

I. INTRODUCTION

Prussian blue analogs (PBAs) have attracted a great deal of interest since high-T_C examples were discovered in 1995 by the Verdaguer group[1] and the subsequent 1996 report of photo-induced magnetization in examples by the Hashimoto group[2]. The latter property opened the possibility of integrating PBAs into magneto-optical devices and provided an important new class of switchable molecular materials[3–7]. While the electronic mechanism involved in the thermally- and photo-induced transitions has been recently elucidated, the associated structural aspects remain relatively unstudied. Short-range structural modifications in $A_xCo[Fe(CN)_6]_y \cdot zH_2O$ (A: alkali metal) PBAs were observed in 1998 by EXAFS[8,9], but complete analysis of the long-range aspects remain to be investigated. These structural modifications are obviously involved in the multistability previously reported for some PBAs[10], and might play a key role in the control of the photo-induced magnetic phases.

The electronic switching in the Co-Fe based PBAs is described as a charge-transfer induced spin transition (CTIST)[2], which occurs between "active" Co-Fe pairs:

$$\underset{\text{(low temperature)}}{Co^{III}\ (S = 0)\text{-}Fe^{II}\ (S = 0)} \leftrightarrow \underset{\text{(high temperature)}}{Co^{II}\ (S = 3/2)\text{-}Fe^{III}\ (S = 1/2)}$$

where the Fe^{2+} to Co^{3+} electron transfer is associated with a low spin (LS) to high spin (HS) transition of the cobalt ion. The electron transfer and spin state change cannot be trivially disentangled, but can be considered as successive steps for the photo-induced transition[11,12]. The condition for a pair to be "active" has been analyzed in terms of the redox potential difference of the metal atoms, and depends on the density of $[Fe(CN)_6]^{3-}$ vacancies in the system[13].

Upon rapid cooling, CTIST PBAs can be quenched and trapped at low temperature in the high-temperature state. Spin crossover (SC) and PBA compounds have provided examples of efficient quenching, which can be obtained when the gap between the thermal transition temperature and the thermal return temperature, often called T_{LIESST}[14] for the SC compounds, is narrow enough to prevent sizable relaxation of the metastable HS state during the cooling process. The ability of such systems to be thermally quenched in the HT state makes it possible to investigate the differences between the thermally quenched and photo-induced metastable states, previously called "multimetastability"[15]. It is also important to recall that the presence of magnetic interactions in PBAs leads to large photo-magnetic effects at low temperature[16–19], so low-temperature magnetic data can be used, as a first approach, for differentiating the various metastable states of the system.

Efficient quenching was recently observed for $Na_{0.32}Co[Fe(CN)_6]_{0.74} \cdot 3.4H_2O$ using magnetic, Mössbauer[20] and calorimetric measurements[21]. The present work extends these studies to the potassium analog, $K_{0.3}Co[Fe(CN)_6]_{0.77} \cdot 4.4H_2O$, which exhibits an "intermediate" state (IM) upon slow cooling below the CTIST temperature. This unusual state has magnetic susceptibility values in-between those expected for the low- and high-spin states, with a large hysteresis[22], the kinetic nature of which is shown in Figure 1. This article reports on photo-magnetic, diffuse reflectance, calorimetric and X-ray diffraction investigations. For convenience, the discussion of structural data is restricted to a comparison of the as-synthesized compound and the IM state, leaving a complete investigation of the structural aspects to follow in a separate report[23].

II. EXPERIMENTAL SECTION

Reagents, Synthesis and Chemical analysis. Chemical precursors were obtained from Sigma-Aldrich and used as received. Deionized water was obtained from a Barnstead NANOpure system. A reddish brown powder was obtained by dropwise combination of three different nanopure water solutions: $Co(NO_3)_2 \cdot 6H_2O$ (0.005mol in 50mL H_2O), $K_3Fe(CN)_6$ (0.02mol in 200mL H_2O) and KNO_3 (0.1mol in 50mL H_2O). The powder was extracted by centrifugation and then dried in vacuum. IR spectra using KBr pellets were recorded on a Thermo Scientific Nicolet 6700 spectrometer in order to characterize the Fe-CN-Co vibration bands: 2155 (vs. ν_{CN}), 2114 (m. ν_{CN}), 2092 (vw. ν_{CN}) cm^{-1}, respectively assigned to Fe(III)Co(II), Fe(II)Co(III), Fe(II)Co(II) pairs[18]. Energy dispersive X-ray spectroscopy (EDS) was conducted on a JOEL 2010F instrument at the Major Analytical Instrumentation Center at the University of Florida, in order to determine the transition metal content (Co/Fe) 56.39/43.57. The K/Co content, ~ 0.27 was inferred from electro-neutrality, using the room temperature valence state $Fe(II)_{0.08}$-$Fe(III)_{0.92}$ from unpublished Mössbauer data, and assuming for chemical reasons that Co is exclusively in the Co(II) state; the K content should be reduced in case of a sizable departure from a mere Co(II) state; note that the presence of a Fe(II)-CN-Co(III) band in the IR spectrum can be assigned to damage due to pellet processing. The C, N, H content was determined by combustion analysis at the University of Florida Spectroscopic Services Laboratory: using an acetone suspension, samples were deposited onto 400 mesh copper grids with ultrathin carbon film on a holey carbon support film obtained from Ted Pella, Inc. Due to the inaccuracies in the K and H contents, the final formulation was expressed as $K_{0.3}Co[Fe(CN)_6]_{0.77} \cdot 4.4H_2O$. Anal. Calcd for $C_{4.6}H_{8.8}N_{4.6}O_{4.4}K_{0.32}Co_{1.0}Fe_{0.77}$: C, 18.66; H, 2.98; N, 21.76. Found C, 18.36; H, 2.06; N, 21.90.

DC-magnetization under 0.1 Tesla applied field was measured by a SQUID magnetometer (Quantum Design MPMS-5) equipped with an optical fiber. Irradiation was provided by a 100 W tungsten lamp with 750nm filter (50nm bandwidth). Typical intensity was $15mW/cm^2$. For the photo-magnetic measurements a thin layer of powder sample was fixed onto a transparent double-stick tape located at the tip of the optical fiber. The complete photo-magnetic system was described in a previous work[24]. The mass of the thin sample (~ 0.64mg) was obtained by comparison to the room temperature data of the bulk sample (18.5mg) used for measurements in the dark, after systematic correction of the diamagnetic contribution of the photo-magnetic sample holder[24]. Susceptibilities were corrected for diamagnetic contributions, by using literature values[25].

Calorimetric measurements were performed using a differential scanning calorimeter (DSC) Q1000 from TA Instruments. The low temperature range was obtained using a liquid nitrogen cooling system allowing reaching and stabilizing 93K in the sample holder. The measurements were carried out using around 4mg of powder sample sealed in aluminum capsules with a mechanical crimp and at a scan rate of 1K/min. The experiment with the quenched

State	T_C (K)	T_{relax} (K)	M_s (emu/g)	B_c (G)	HS content (%)
Q (bulk sample)	14	160	not meas.	not meas.	85
Q (layer sample)	11	159	6.62	60	55
LT	-	-	-	~ 0	~ 0
IM (layer sample)	~ 11	-	4.00	60	25
LTPX(layer sample)	18	$130 - 140$	8.17	830	~ 50
IMPX (layer sample)	17	130&$150 - 170$	10.49	660	~ 60

TABLE I: Properties of the Q, LT, IM, LTPX and IMPX states, derived from magnetic data. T_C is the magnetic ordering (freezing) temperature determined as the inflection point of the low-temperature M(T) curves. T_{relax} is the thermal relaxation temperature determined as the inflection point of the χ_m·T(T) curve during the thermal decay of the metastable state. M_s is the zero-field extrapolated value of the M(H) curves, with B_c the coercive field. The low-temperature HS content was estimated by comparing the χ_m·T values in the low-temperature plateau with those above the CTIST.

sample was performed after immersing the capsule into liquid nitrogen followed by rapid transfer to the DSC cryostat, opened at 93K under a flow of helium gas. The calibration procedure was already reported in Ref. 21.

The diffuse reflectance device was described in Ref. 26. The irradiation system was the same as that used for the photo-magnetic measurements.

The synchrotron x-ray powder diffraction (XPD) measurements were performed at Swiss-Norwegian Beam-Lines (station BM1A) at the European Synchrotron Radiation Factory (France). The powder sample was sealed in a 0.1-mm diameter Lindemann glass capillary. The diffraction patterns were collected with an imaging plate detector by exposing the sample for 90 seconds to a monochromatic x-ray beam, $\lambda = 0.72689\mathring{A}$. The as-grown sample was fine enough and gave a homogeneous intensity distribution in the Debye-Sherrer rings. LaB_6 standard powder (NIST) was used to calibrate the sample-to-detector distance, the beam center and the tilt angle of the image plate detector. For the temperature-dependent measurements, an Oxford Cryostream N_2 blower was used for temperature control between 80K and 300K. For quenching, the sample was directly cooled to 80K from room temperature. The spontaneous charge-transfer transition and thermal relaxation processes were investigated with 1K/min sweep rate.

III. RESULTS AND DISCUSSION

A. Magnetic measurements

The temperature dependent magnetic response measured in the dark is shown in Figure 1. The sample was rapidly cooled down to $\sim$ 50K by fast insertion into the pre-cooled sample space of the SQUID magnetometer to achieve the quenched state. It was subsequently warmed (1 K/min) until thermal relaxation was complete ($\sim$ 200K) and then cooled again to achieve the LT state, before rewarming to record the spontaneous CTIST, observed here at 230K (inflection point of the χ_M·T(T) curve). The unusual onset of an intermediate low-temperature state (IM), reported by Park et al.[22] was reproduced upon slow cooling and was shown to be sizably dependent on the temperature scan rate. The slow evolution of the system below the CTIST explains why the thermal quenching process is rather efficient in spite of the wide temperature range which separates the CTIST temperature ($\sim$ 230K) and the thermal return temperature ($\sim$ 160K), Figure 1. As it will be shown in the following, the amount of HT state trapped by rapid cooling sensitively depends on the heat capacity of the sample holder. Furthermore, detailed X-ray synchrotron investigations of the system[23] confirmed that the first quenching was virtually complete, but following cycles were not, suggesting some fatigue of the sample generated by the successive thermo- and photo-switching experiments. A similar ageing effect was observed on the Na-compound, presumably arising from the large volume change, $\Delta V/V \sim 9\%$, which accompanies the spin transition.

Using a thin-layer sample fixed on the tip of the sample holder, we repeated identical sequences to form the low-temperature states: quenched (Q), relaxed quenched (LT) and slowly cooled (IM) states. Photo-excitation was performed at 6K at 750nm, 15mW/cm^2, for 3 hours starting either from the LT state or from the IM state to produce the LTPX and IMPX states, respectively (PX indicates a photoexcited state). We first recorded the thermal variation of the resulting magnetic moment in the $6 - 40$K temperature range to measure the "magnetic ordering temperature" (actually the spin-freezing temperature of the cluster-glass state[19], Figure 2.

The M-H scans were then recorded at low temperature (6K) to determine the saturation magnetization and coercive field values of the system, Figure 3. Finally the sample was warmed at constant scan rate (1K/min) to determine the thermal return temperatures of the different metastable states, Figure 4.

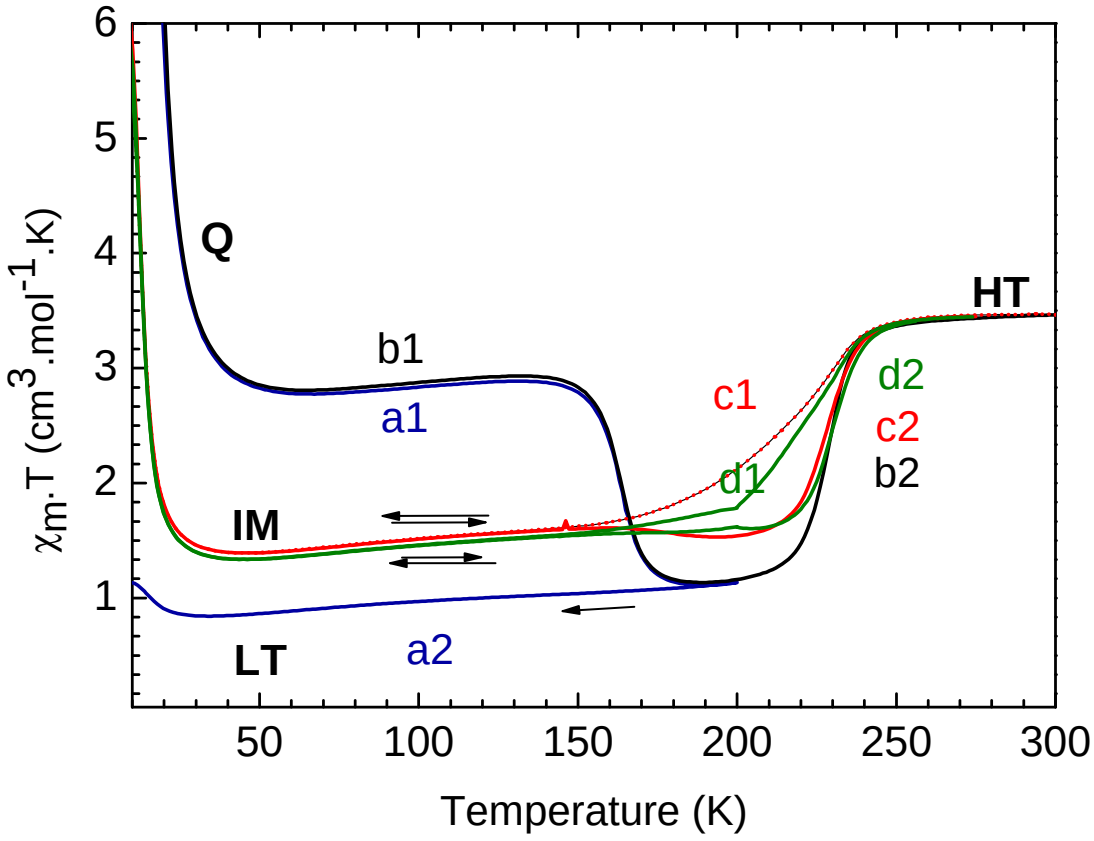

FIG. 1: Temperature dependences of the χ_m·T product, obtained with the bulk sample under 0.1 Tesla applied field. Blue (a) and black (b) curves start from the thermally quenched state. The red (c) and green (d) curves start from room temperature, at a controlled temperature scan rate: 1 and 0.1K/min, respectively. The different low-temperature states are labeled Q (after thermal quenching), LT (after relaxation of the Q state) and IM (intermediate state). Color on line.

The main data derived from Figures 1, 2, 3, 4 have been summarized in Table I. The qualitative findings are: (i) Neither the quenching nor the photo-excitation processes are complete. The lower efficiency of the quenching process with respect to the bulk sample (Figure 1) is explained by the impact of the heat capacity of the sample holder upon the effective cooling rate. On the other hand, the HS content of the IM state in both samples is the same. (ii) The magnetic properties of the Q-state sizably depend on the HS content. (iii) The IM state has magnetic properties similar to those of the Q state with 55% HS content. (iv) The Q and LTPX states clearly decay to the same LT state (this result was confirmed by synchrotron XRD, see Ref. 23). (v) The thermal decay occurs more progressively for the photoexcited (PX) states than for the Q state. (vi) The decay of the IMPX state occurs in two steps, suggesting that the initial system is somehow heterogeneous. (vii) The decay of the IMPX state is not complete when the system reaches the CTIST temperature upon warming.

B. Magnetic properties of the Q and LTPX states

It is worth considering the incomplete population of the HS state in the Q and LTPX states, and its impact on the magnetic and relaxation properties. Due to the long life time of the PX states at low temperature, it must be considered that photo-excitation is a frontal process mainly limited by the bulk absorption of light in these highly colored samples. This leads to a non-homogenous state of the sample, with a front part almost saturated, leaving part that is almost non-excited[3,4]. The situation is quite different for the Q state, the incomplete character of which results from partial relaxation occurring at intermediate temperatures during the cooling process. In the case of

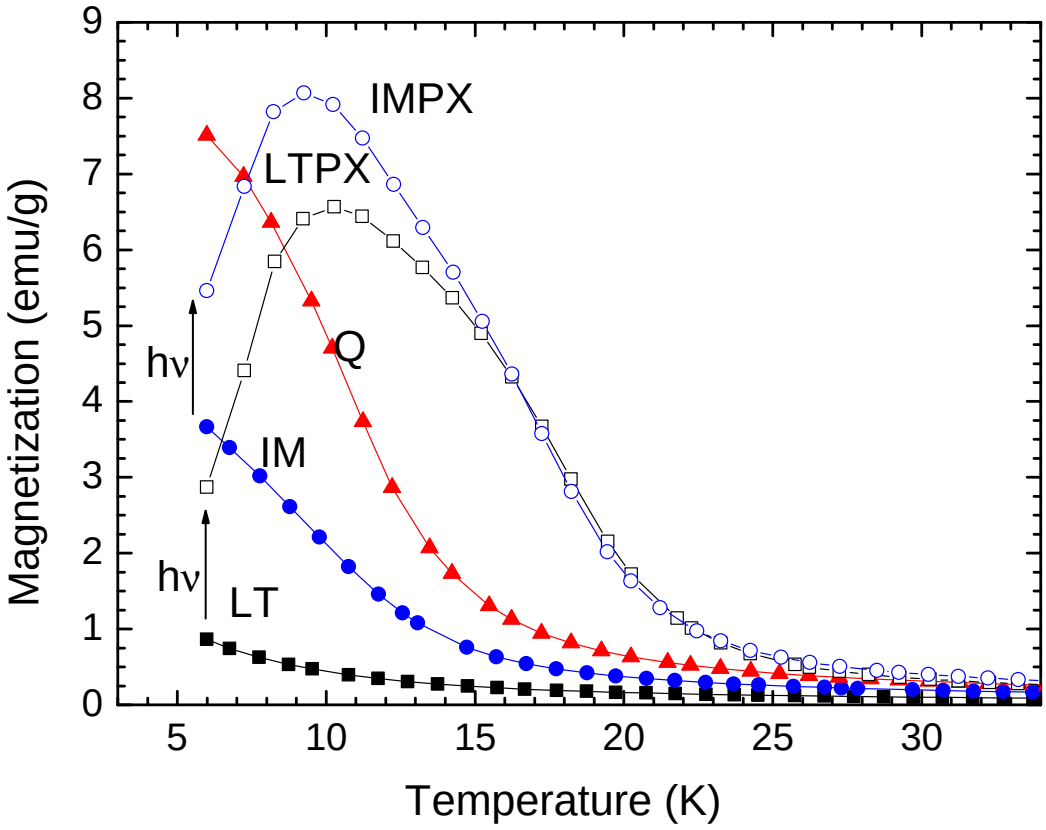

FIG. 2: Low-temperature magnetization curves of the layer sample, recorded after rapid (Q state) or slow (IM state) cooling, or after photo-excitation (LTPX, IMPX states). The applied field was 0.1 Tesla. The low-temperature increase of the LTPX and IMPX curves may be assigned to the non-relaxed character of the "raw photo-induced" state of the system which departs from the usual field-cooled state[27,28]. Magnetic freezing temperature values, T_C, are listed in Table I.

a distribution of energy barriers, as reported for the Na-analogue[20], relaxation proceeds faster with the switchable pairs having the lower energy barriers. Consequently, the final Q-state preferably contains pairs having high energy barriers. Such selectivity could slightly impact the thermal relaxation temperature[29–31], but this effect is not reflected in the experimental data listed in Table I. Also, the magnetic ordering temperature is expected to be sensitive to the HS content, and indeed this effect is observed here (Table I). Using a rough linear extrapolation, which overestimates the result due to the usual shape of the magnetic dilution phase diagrams, we assign the value of $T_C \sim 15.5$K to a hypothetical 100% quenched state. On the other hand, the T_C value assigned to the PX state, $T_C \sim 18$K, is certainly underestimated due to the incomplete transformation of the "almost saturated" fraction. Therefore, this analysis suggests a sizable difference between the T_C values of the Q and LTPX states, below 16K and above 18K, respectively.

The present data for the Q and LTPX states qualitatively agree with the previous observations made for the Na-compound[10]. The Q state possesses a lower T_C, a higher T_{relax} and a smaller M_s values for comparable HS fraction. Also, according to the detailed structural investigation[23], the unit cell parameter has a smaller value in the Q state. The Q state is isostructural with the high-temperature phase (cubic, $Fm\bar{3}m$ space group), and a recent X-ray investigation[32] suggested that the LT phase has lower (rhombohedral) symmetry than the high-temperature phase. Following the textbook example of $Fe(ptz)_6$ - based SC compounds[33] it is generally assumed that photo-excitation at low temperature does not induce structural changes (although counter-examples seem to be provided by compounds possessing flexible ligands[29–31]). These two considerations led us to the simple idea that the decay of the Q-state involves both electronic and structural transformations, while the decay of the LTPX state only involves an electronic transformation.

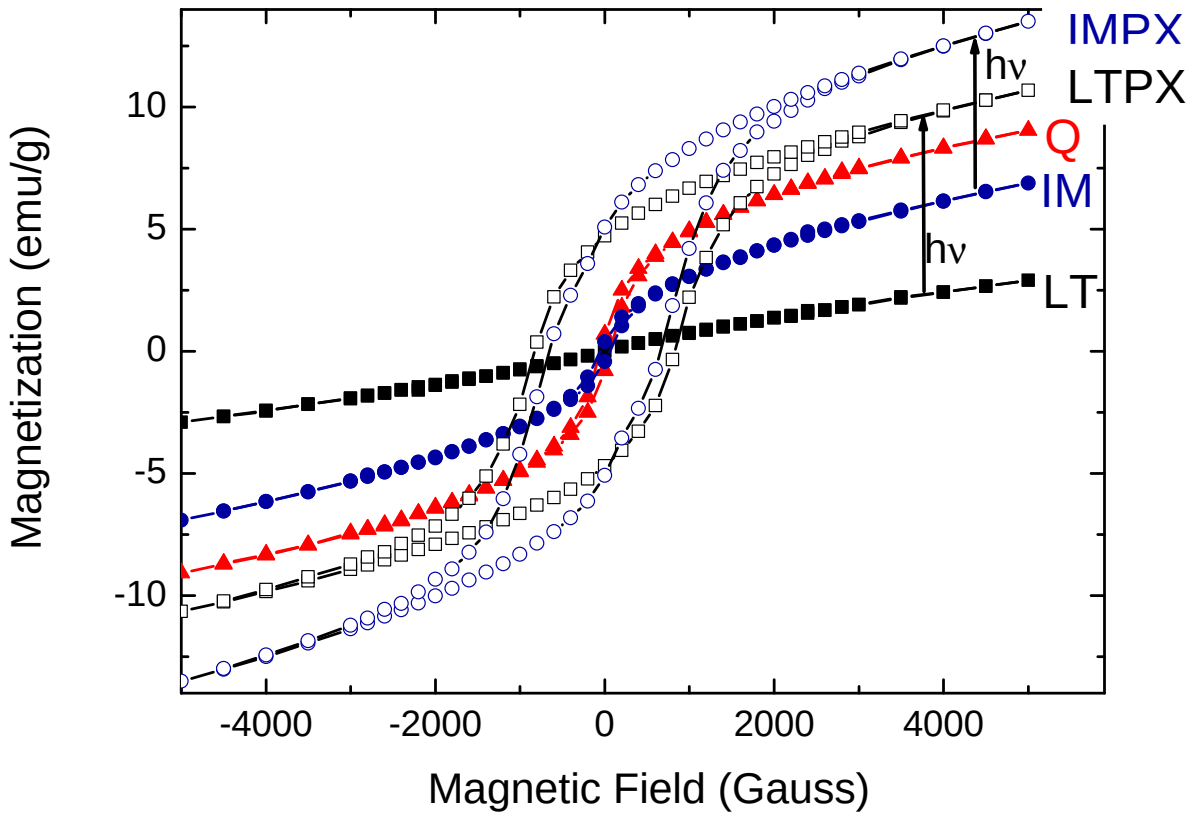

FIG. 3: M-H curves measured at 6K, of the thin-layer sample.

C. Thermal decay of the Q and LTPX states

In the experimental curves reported in Figure 4, the difference in the thermal decay temperatures is assigned to the presence (Q state) or absence (LTPX state) of this structural transformation. This suggestion is supported by the fact that the decay temperature of the Q-state does not sizably depend upon its HS content. The presence of a structural difference between the Q and LTPX states will also impact the isothermal relaxation curves reported, below. It is also noteworthy that during the low-temperature photo-excitation process, all lifetimes are long and there is no selectivity among states with different energy barriers. This absence of selection may contribute to the slight smearing of the thermal decay curve of the LTPX state.

D. Nature of the IM state

A crucial experimental feature is the two-step character of the decay of the IMPX state, see Figure 4. These steps roughly coincide with the thermal return temperatures of the LTPX and Q states. It is therefore suggested that the IM state is a mixture of Q and LT-like fractions. This simple model is supported by the shapes of the M(T) curve and M vs H loop of the IM state, which are strikingly similar to those of the partially relaxed thin film-based Q state. Both experimental curves can be fairly well reproduced by linear combinations of the Q and the LT state data, in respective proportions 42 : 58 for the M(T) curve and 62 : 38 for the M(H) curve. These proportions lead to final estimates of the HS fraction in the IM state, of 23 and 34% which roughly agree with the magnetic data derived from Figure 1 and listed in Table I. The difference between these estimates presumably results from the neglect of possible interactions between the Q-like and LT fractions.

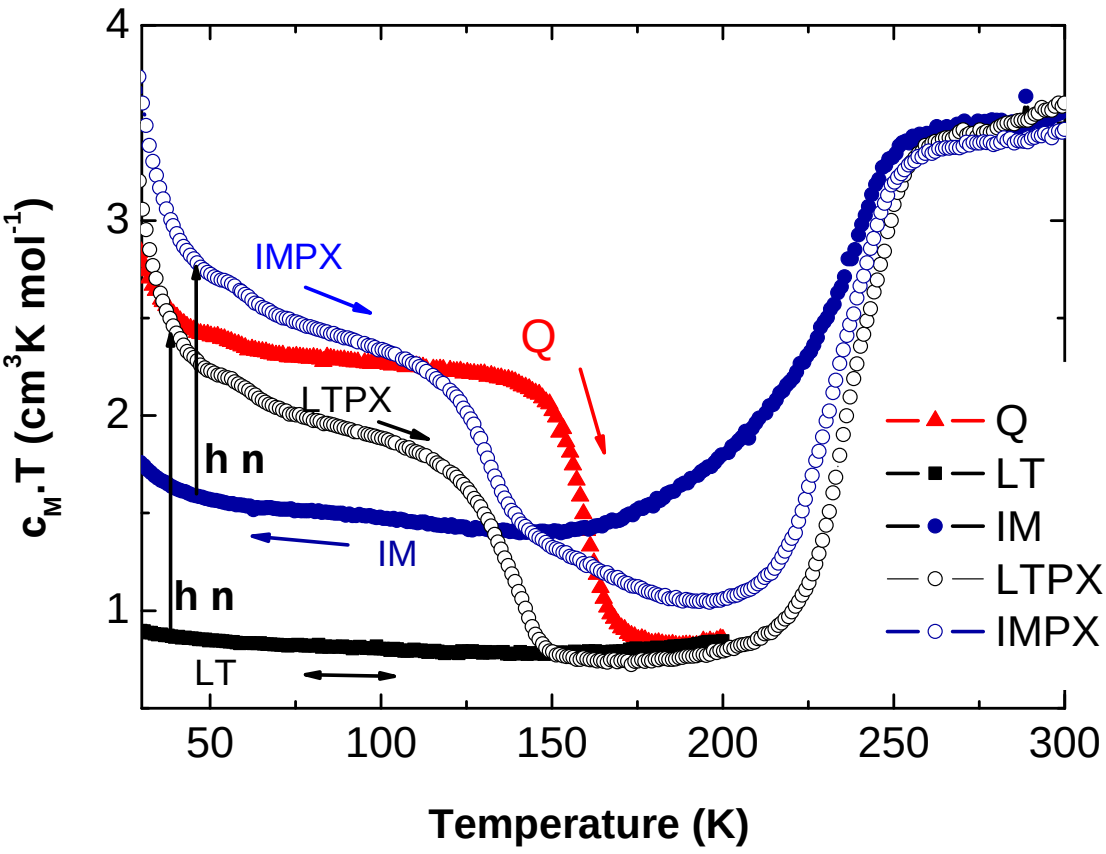

FIG. 4: Temperature dependences of the χ_m·T product obtained with the thin-layer sample under 0.1 Tesla applied field. The photoexcited states were obtained after irradiation at 750nm at 15mW/cm^2 for 3 hours, starting from the LT state (LTPX curve) or from the intermediate state (IMPX curve). Temperature scan rate was 1K/min.

It is worth noting that the second step of the decay of the IMPX state is smeared out over a broad temperature range, from $\sim$ 150K to $\sim$ 200K. This effect can be assigned to local inhomogeneities, the nature of which will be discussed further below in the context of the diffraction data. At first glance, one might expect that IMPX should return to its initial IM state (LT + Q) after the first relaxation stage (LTPX $\rightarrow$ LT). However the second stage, where the Q-type fraction relaxes, takes place more efficiently than for the initial IM state, an effect attributable to physical ageing of the IM state.

E. Isothermal relaxation of the Q and LTPX states

The isothermal relaxation curves of the Q state, recorded with the bulk sample, are shown in Figure 5. The data are normalized to the low-temperature value of the quenched HS fraction that is close to 1 at t = 0. The isothermal relaxation curves of the LTPX photo-excited state are shown in Figure 6. These have been rescaled to the initial value of 1 for simplicity, as their almost single exponential character makes the parameters nearly independent of the scaling factor.

The shapes of the relaxation curves for the Q and LTPX states reveal qualitative differences, since the Q-state curves exhibit a marked sigmoidal shape. However both exhibit long relaxation tails which usually can be assigned to distributions of relaxation times[34], or alternatively to the onset of correlations associated with short range interactions[35]. To provide a further insight into these alternative assumptions, we apply here a model accounting for correlations[36]. We recall that the simple cooperative 2-level relaxation model based on the mean-field approach, and using the Hauser

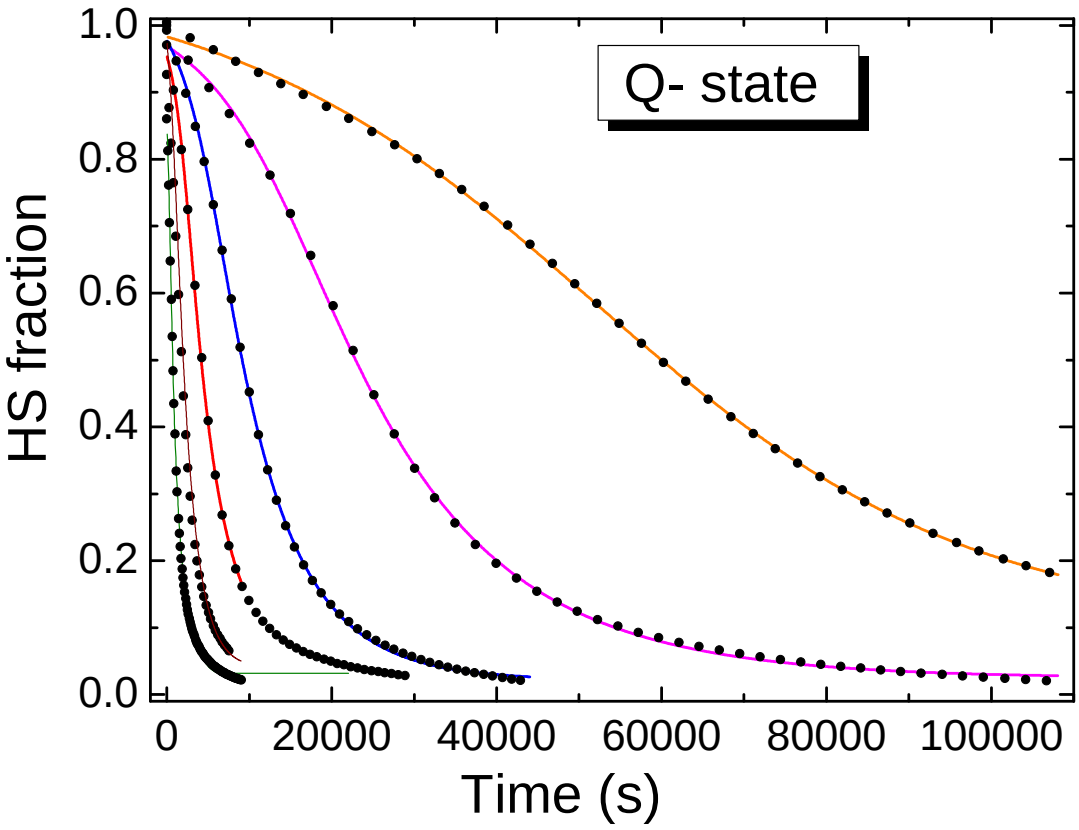

FIG. 5: Isothermal relaxation curves for the Q-state at 155, 150, 145, 140, 135, 130K, from left to right, with best-fit computed curves.

self-acceleration factor[37] $k_{HL}(T,n_{HS})= k_\infty \exp(-E_a^0/k_BT)\exp(-\alpha(T)n_{HS})$ where $\alpha = 2zJ/k_BT$, conveniently reproduces the sigmoidal shape of the relaxation curves until $n_{HS} \sim 0.5$, but fails to overlap the long relaxation tails. As shown in Figures 5, 6 and 14 these tails are accurately reproduced by the correlation model used here.

The two-variable correlation model of Ref. 36 is based on the pair approximation method which includes short-range fluctuations of the Co^{2+}(HS)-Fe^{3+} fractions by explicitly taking into account short-range correlations. The stochastic treatment of this problem yields two coupled differential equations governing the HS fractions, $n_{HS}(t)$, and the fraction of HS-LS pairs, denoted $n_{HL}(t)$, where HS is representative of the Co^{2+}-Fe^{3+} pairs and LS the Co^{3+}-Fe^{2+} pairs. We show here for simplicity the shorter expressions suitable for the HS $\rightarrow$ LS relaxation process:

$$\frac{dn_{HS}}{dt} = -\frac{n_{HS}}{2\tau_0} e^{-\beta\left(E_a^0 + J(2n_{HS}-1) - \Delta + 1/2k_BTln(g)\right)} \times \left(e^{-\beta J_{short}} + 2\frac{n_{HL}}{n_{HS}} sinh(\beta J_{short})\right)^q \quad (1)$$

and

$$\frac{n_{HL}}{dt} = -\frac{n_{HS}}{2\tau_0} e^{-\beta(E_a^0 + J(2n_{HS}-1) - \Delta + 1/2k_BTln(g))^{q-1}} \times \left(e^{-\beta J_{short}} + 2\frac{n_{HL}}{n_{HS}} cosh(\beta J_{short})\right) \times \left(e^{-\beta J_{short}} + 2\frac{n_{HL}}{n_{HS}} sinh(\beta J_{short})\right)^{q-1} \quad (2)$$

with β=1/k_BT and J and J_{short} are the long- and short-range interaction parameters, taken here as temperature independent for simplicity; q is the connectivity of the system, taken here equal to 4 considering the partial occupancy

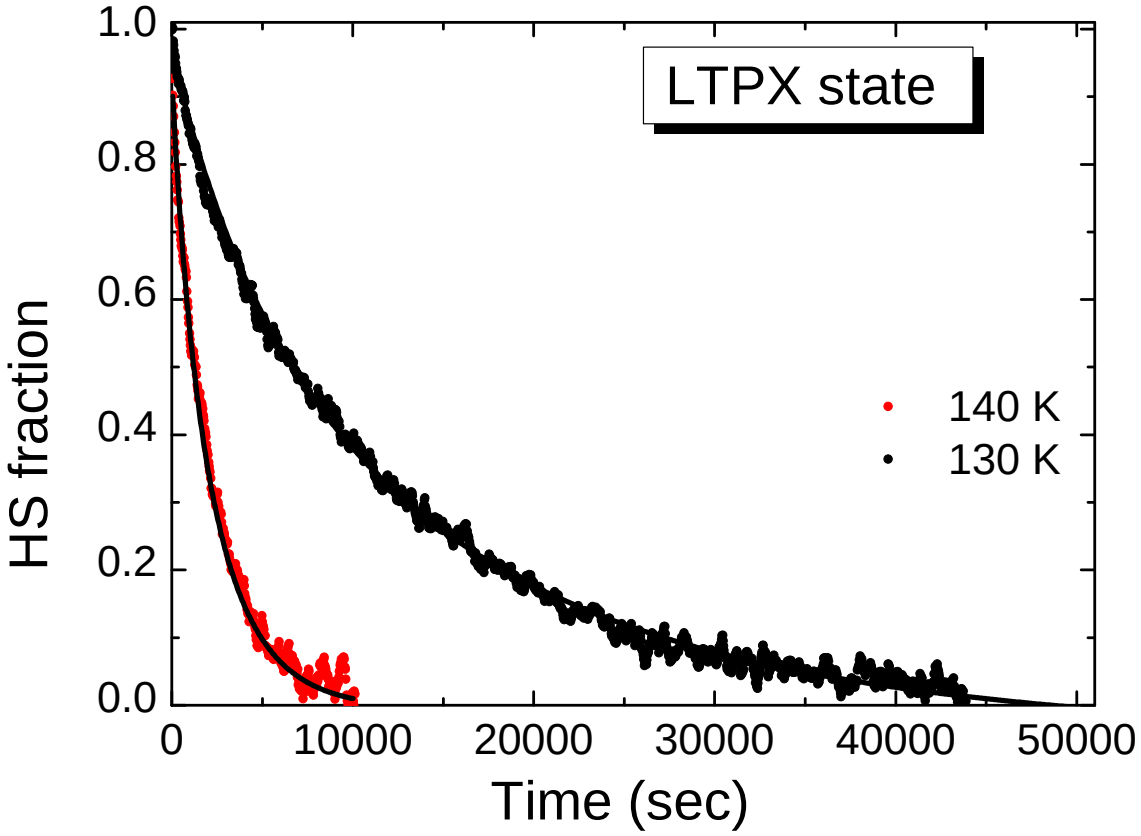

FIG. 6: Isothermal relaxation curves for the LTPX state at 130K (black symbols) and 140K (red symbols), with best-fit computed curves. The noise in the relaxation data, despite a preliminary smoothing over 10 neighboring values, is due to the very small sample mass used for the photo-magnetic measurements.

(0.77) of the Fe sites in the 3D lattice and accounting for (unpublished) Mössbauer data which show that only $\sim 80-90\%$ of the iron atoms participate in the charge-transfer process. E_a^0 (noted E_a in the following) is the activation energy of the symmetrical double-well system and the frequency factor, $1/\tau_0$ is equivalent to k_∞ (given in Hauser equation). 2Δ is the energy gap and g is the effective degeneracy ratio of the HS/LS states, determined from calorimetric measurements as $\ln(g) = \Delta S / R$ where R is the gas constant. When the above equations are completed with the LS $\rightarrow$ HS process the model also provides the quasi-static behavior of the system at the thermal transition. Fits to the relaxation curves based on the above equations are shown in Figures 5, 6 and 14, and the fitting parameters are listed in Tables I and IV. To get better agreement we also introduced a multiplicative scaling factor and a "residual" value of the HS fraction, which mainly compensates for minor errors of the normalization procedure of the experimental data. The fitted data reveal an unexpected thermal variation which will be addressed in the discussion section in the light of the relaxation data obtained with the Na-analogue.

The values of E_a and τ_0 were determined by refining an Arrhenius plot of the values obtained at different temperatures for the frequency factor $(1/\tau_0)\ \exp(-E_a/k_BT)$. We obtained $E_a = 4850$ (200)K, with the frequency factor $\ln(1/\tau_0) = 23.(2)$ leading to $1/\tau_0 \sim 1.0 \times 10^{10}\ s^{-1}$. It is worth remembering that the barrier selectivity associated with the quenching process is expected to slightly overestimate the frequency factors, and the data for the PX state lead to slightly smaller values $E_a = 4610$K and $1/\tau_0 \sim 2.8 \times 10^9\ s^{-1}$.

The data derived from the relaxation of the Q state reproduce the CTIST properties rather well, as shown in Figure 7 (curve Q). The problem of the quantitative consistency between the relaxation and thermal transition data previously addressed[20] seems to have a minor impact here. The quasi-exponential relaxation data of the LTPX state does not lead to a cooperative thermal transition. For the needs of the coming discussion, we also present in Figure 7

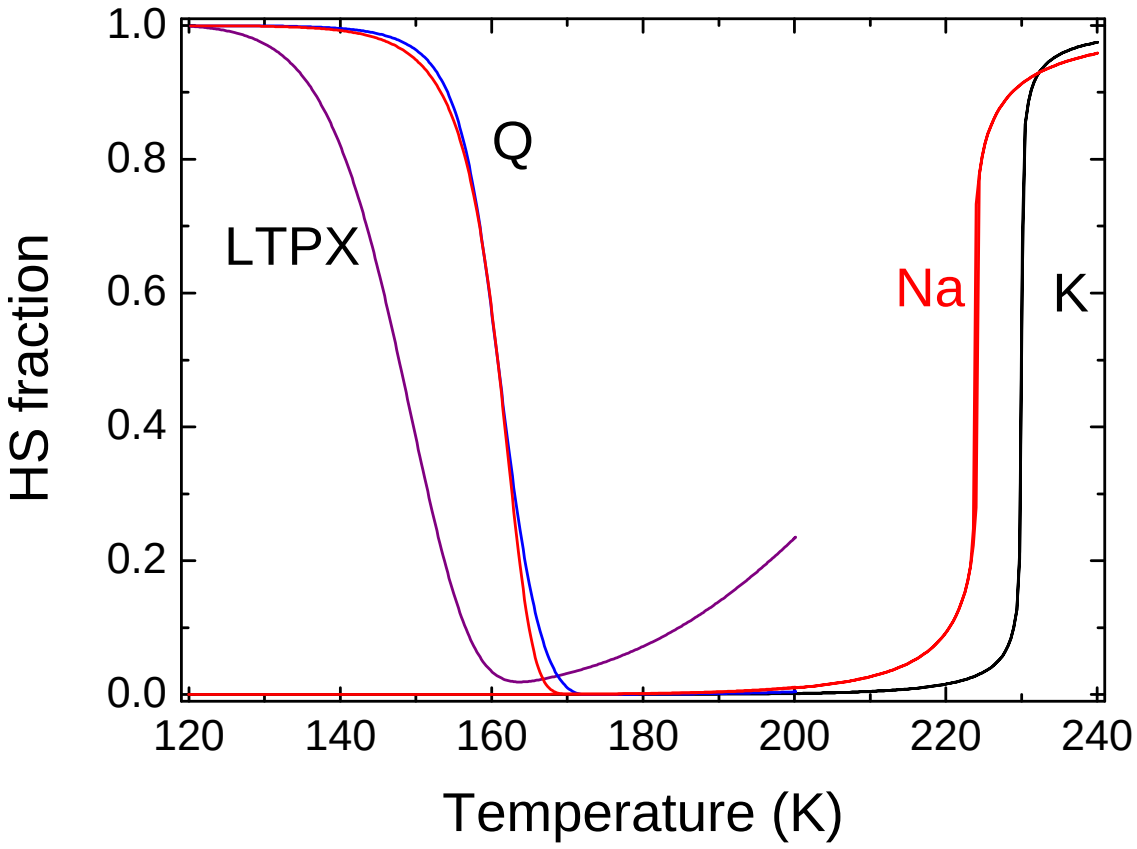

FIG. 7: Computed thermal relaxation and thermal transition curves of the K-compound, using kinetic and interaction parameters derived from the analysis of the relaxation curves (black full lines). The red line corresponds to the Na-analogue data. The energy gap values have been determined (3450, 2688K for the K-, Na-compounds respectively) so as to match the experimental transition temperature ranges. Color on line.

the transition curve computed in a similar way, that is, using the relaxation data of the Q-state, for the Na-analogue, which does not reproduce the $\sim$ 20K-wide experimental hysteresis.

Finally, we briefly address the problem of the energy barrier distributions. In previous work[20] using a spin-crossover compound[29–31] we demonstrated that ligand field distributions efficiently compete against the interaction parameters, and reduce the effective cooperativity of the system, manifested in the sigmoidal character of the relaxation curves and the width of the thermal hysteresis loop. As for the Na-analogue, a distribution of energy gaps can be assigned to different $CoN_{6-x}O_x$ environments known to exist in the K-compound, associated with the change in ligand field strength on H_2O substitution and possible local distortions generated by the random occupancy of the $Fe(CN)_6$ sites. However, these distributions are also present in the Q state and would hardly explain the striking difference between the relaxation of the Q and LTPX states. Instead, we assign this difference to the structural change which occurs during the decay of the Q state.

F. Calorimetric data

DSC measurements at 1K/min upon cooling from room temperature and subsequent heating are reported in Figure 8. They refer to the HT $\leftrightarrow$ IM transformation and show atypical features. The C_p anomaly on cooling is significantly smaller than the one on heating, and below the temperature of the anomaly, the slope of the cooling branch is much different from that of the heating branch. These features agree with the non-equilibrium character of the HT $\leftrightarrow$ IM transformation as suggested by the kinetic effects seen in Figure 1. Also, the cooling curve is single-peaked, while the

State	T(K)	$1/\tau_0$ (s^{-1})	J (K)	J_{short} (K)	Scaling factor	HS residual
Q	130	0.246×10^{11}	−2.1	64.9	0.853	0.135
	135	0.301×10^{11}	−57.2	105	0.946	0.024
	140	0.276×10^{11}	−72.7	109	0.954	0.021
	145	0.289×10^{11}	−88.1	127	0.919	0.032
	150	0.203×10^{11}	−84.8	114	0.910	0.052
LTPX	130	0.539×10^{11}	−55.4	0	1.02	−0.05
	130	0.551×10^{11}	0	−12.1	1.01	−0.04
	140	0.436×10^{11}	−26.7	0	0.93	0.07
	140	0.438×10^{11}	0	−6.2	0.93	0.07

TABLE II: Refined parameters for the isothermal relaxation curves of $K_{0.3}Co[Fe(CN)_6]_{0.77}\cdot 4.4H_2O$ shown in Figures 5 (Q state) and 6 (LTPX state), using the two variable correlation model[36] (due to the tight correlation between E_a and τ_0 parameters, the fixed value $E_a = 5000$K was used to make τ_0 values essentially independent of temperature. The crude choice of E_a has no impact on the other parameters).

heating branch appears doubly stepped. The data obtained starting from the quenched sample is reported in Figure 9. The decay of the Q-state is also single peaked, but the peak of the LT → HT transition is again multi-stepped. The quantitative data are summarized in Table III and reveal that the ΔH of the IM → HT transformation is roughly half of that measured at the LT → HT transition, which is consistent with the description of the IM state in terms of a nearly equal mixture of Q and LT states. Also, ΔH of the Q → LT transformation is much less than for the LT → HT transition, due to the incomplete character of the quenching process (∼ 50% yield). The C_p peak on heating occurs at ∼ 160K, which agrees with the value ∼ 159 − 160K determined by magnetic measurements at the same scan rate.

The complex shapes of the C_p anomalies of the LT → HT and IM → HT transitions agree with the idea that multi-scale processes take place involving both electronic and structural transformations, and that other factors are also at play, such as internal stresses created by the large volume change upon the CTIST transition ($\Delta V/V \sim 9\%$). However the Q → LT transformation, which also involves both processes, does not result in such a complex shape of the C_p anomaly. We imagine that the various factors involved in these two kinds of solid-state transformations may differ, due to the different temperatures at which these transformations take place. Also the impact of defects which can hinder electron transfer may depend upon temperature.

According to Table III, the measured ΔH and ΔS values for the LT → HT transition are ∼ 25% larger than for the Na-analogue, despite a similar proportion of active Co-Fe switchable pairs (∼ 80% in both cases according to the Mössbauer data). This presumably results from a larger contribution of the structural processes. As in previous work[21] we determined the entropy change associated with the complete switching of a mole of Co-Fe pairs as ΔS(corrected) = ΔS(meas)/0.77/0.8 ∼ $125 JK^{-1}mol^{-1}$ per mole, leading to the degeneracy factor value ln(g)=ΔS/R∼ 15 to be used in the Ising model calculations. Accordingly, the value of the electronic gap in the model may be derived from the ΔH value reported to one mole of switchable pairs, $2\Delta \sim \Delta H(\text{corrected})/R = 3510$K.

	HT → IM	IM → HT	Q → LT	LT → HT
T_m (K)	230	230 − 235	160	235
ΔH ($kJ\cdot mol^{-1}$)	≈ 3	8.7	7.1	18.0
ΔS ($J\cdot mol^{-1}\cdot K^{-1}$)	≈ 13	37.3	44.5(⋆)	76.2

TABLE III: Characteristic temperatures (T_m), enthalpy (ΔH) and entropy (ΔS) values determined from the calorimetric measurements corresponding to the CTIST (IM ↔ HT and LT ↔ HT) and relaxation (Q → LT) transitions. (The starred value ΔS (Q → LT) includes entropy creation due to irreversibility).

G. Diffuse reflectance

The powder sample was initially cooled within a few hours in the dark down to 80K and then irradiated overnight at 750nm. We then recorded the diffused intensity under constant irradiation for temperature sweeps up to room temperature and then back to 80K, at scan rates close to 0.2K/min (Figure 10). The data reveal striking features: (i)

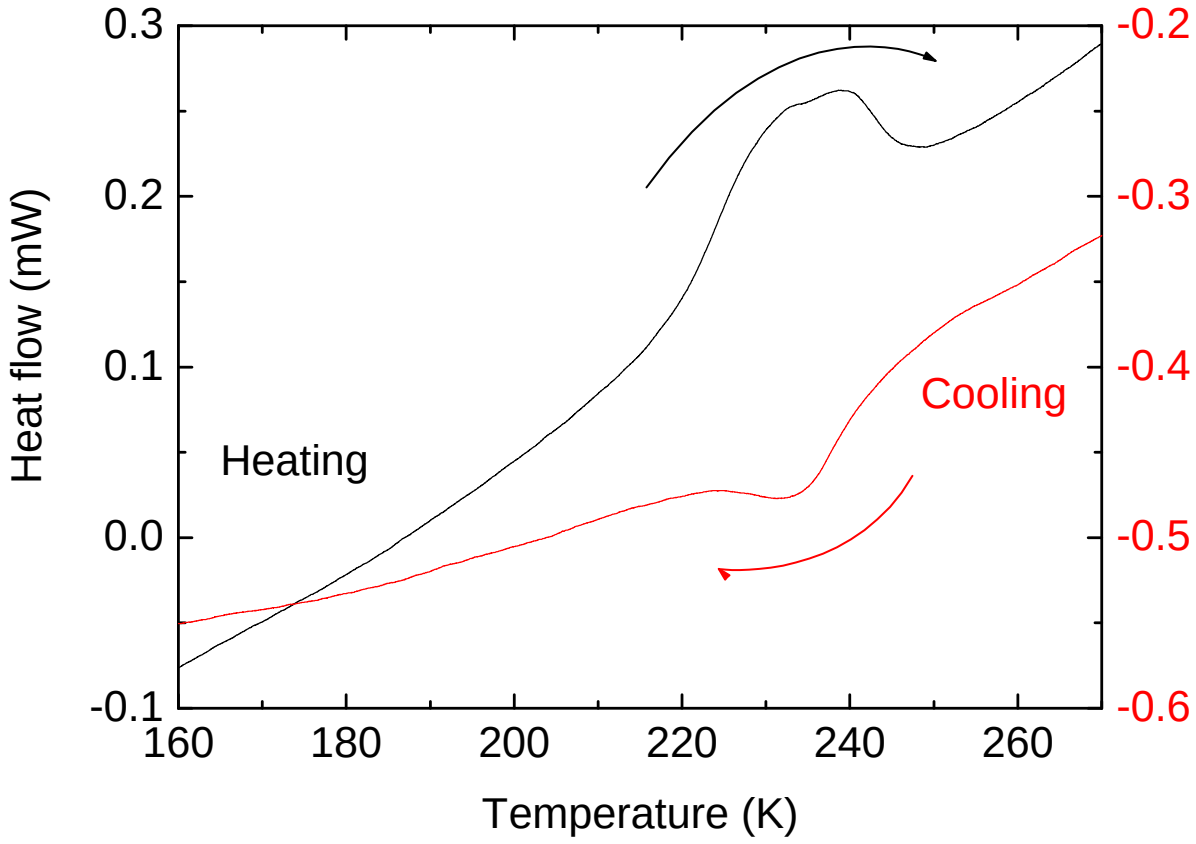

FIG. 8: DSC measurements performed at 1K/min: cooling from room temperature and subsequent heating, associated with the HT ↔ IM transformation.

a drastic reduction of the kinetic effect associated with the onset of the IM state; (ii) the presence of a light-induced thermal hysteresis (LITH)[14,38,39] at lower temperature, revealing that cooperative relaxation efficiently competes against photo-excitation, and (iii) the coincidence of the heating and cooling branches in the plateau temperature interval (150 − 200K). It should be kept in mind that we previously concluded that the LT state was obtained after the decay of both IMPX and LTPX states. Consequently the heating branch of the plateau has to be assigned to the LT state. However, it overlaps the cooling branch which was expected to be in the IM state. To elucidate the possible role of light in these experiments, we performed snapshot measurements which minimize the impact of light on the photo-switchable samples (Figure 11). We compared two sets of data, on cooling, starting from either the HT or from the LT state. It is shown that cooling in the dark from the HT state effectively induces the IM state, although the difference with the LT state is smaller than expected from the magnetic measurements.

Due to the small difference in reflectance observed for the IM state in the dark and the plateau values in Figure 11, we suggest that light may hinder the onset of the IM state. Also, the reduction of the kinetic hysteresis of the thermal transition, relative to the magnetic measurements in the dark, might reveal a light-induced acceleration of the HT → LT relaxation, a point which is addressed further in the discussion section.

H. X-ray diffraction data

We focus here on the properties of the IM state. A more complete structural analysis of the multistable states will be reported separately[23]. Figure 12 shows a typical diffraction pattern of the IM state, taken at 80K on cooling. The IM lines are split into a broad component, here labelled IM(A) and a narrow component, IM(B), establishing the biphasic character of the IM state. The observed phase separation is specific to the slowly cooled IM state, and it

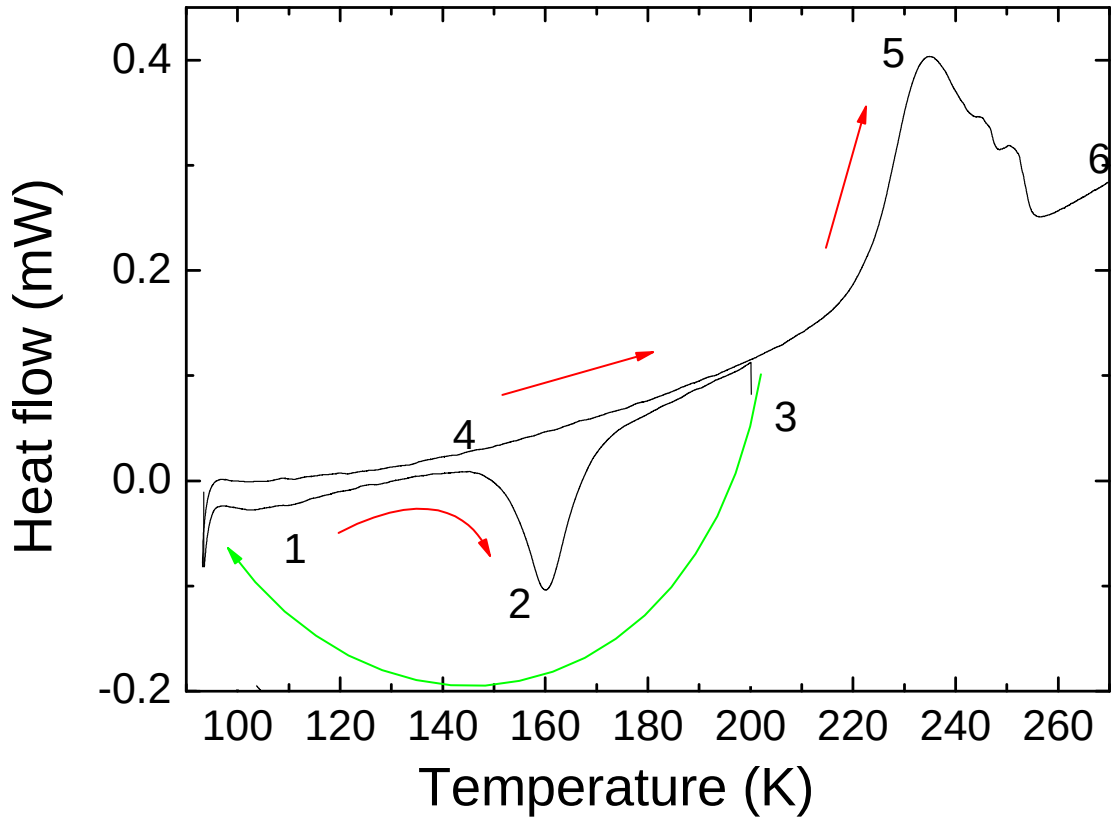

FIG. 9: DSC measurements performed at 1K/min: starting from externally quenched sample, associated with the Q → LT (1 to 3) and LT → HT (4 to 6) transformations.

is worth noting that all other states except the IMPX state, exhibit a single pattern with narrow lines, typical for a homogeneous single phase materials. The lattice parameter of the broad component, IM(A), is 10.095$\mathring{A}$, corresponding to a $\sim 48:52$ mixture of HS and LS states, based on the Q state (10.263$\mathring{A}$ at 80K) and LT state (9.937$\mathring{A}$ at 80K) parameters, whearas the narrow peak labelled IM(B) corresponds to a lattice constant of 9.979$\mathring{A}$, which is close to that of the LS state. The diffraction data unambiguously assign the A and B fractions to the partially relaxed Q (with $\sim 50\%$ HS fraction) and LT states, as already suggested by the magnetic data. The broad character of the IM(A) lines results from a distribution of HS and LS sites in this phase. The slight increase of the lattice parameter values of the IM(B) lines with respect to the pure LT state can be attributed to elastic interactions between micro-phases. The Q:LT proportions are $\sim 60:40$, in rough agreement with the magnetic data. It is important to note here that the HS content of the Q state, as well as the composition of the IM state, sensitively depends on the cooling rate, and may differ between the X-ray experiment, which employs faster cooling, and the photo-magnetic experiments.

In a further step, we systematically analyzed the patterns using Gaussian line shapes and interpreted the data using the Stokes and Wilson formula[40,41]: $(\beta \cdot cos(\theta))^2 = (2 \cdot \eta \cdot sin(\theta))^2 + (\lambda/\epsilon)^2$, where β and 2θ are the width and positions of the diffraction lines, and η and ϵ are the heterogeneity ratio and coherence length value. The unknown parameters η and ϵ are determined by linear regression of the experimental plots of β cos(θ) vs sin(θ). The peak broadening is given by $\beta^2 = \beta_{exp}^2 - \beta_0^2$, where β_{exp} and β_0 are the experimental peak widths and those of a reference sample (LaB_6 NIST standard) averaged over the same θ-interval. The resulting values are reported in Figure 13, together with the variations of the lattice parameters and the proportions of the A and B components. The IM(A) phase has a coherence length of $\sim$ 50nm at 180K, corresponding to $\sim$ 50 unit cells, and is more cluster-like than the IM(B) phase, with a coherence length of $\sim$ 200nm through the whole temperature range. The former values compare to those previously reported upon rapid cooling of the sodium analogue, $Na_{0.42}Co[Fe(CN)_6]_{0.78} \cdot 4.64H_2O$, which were

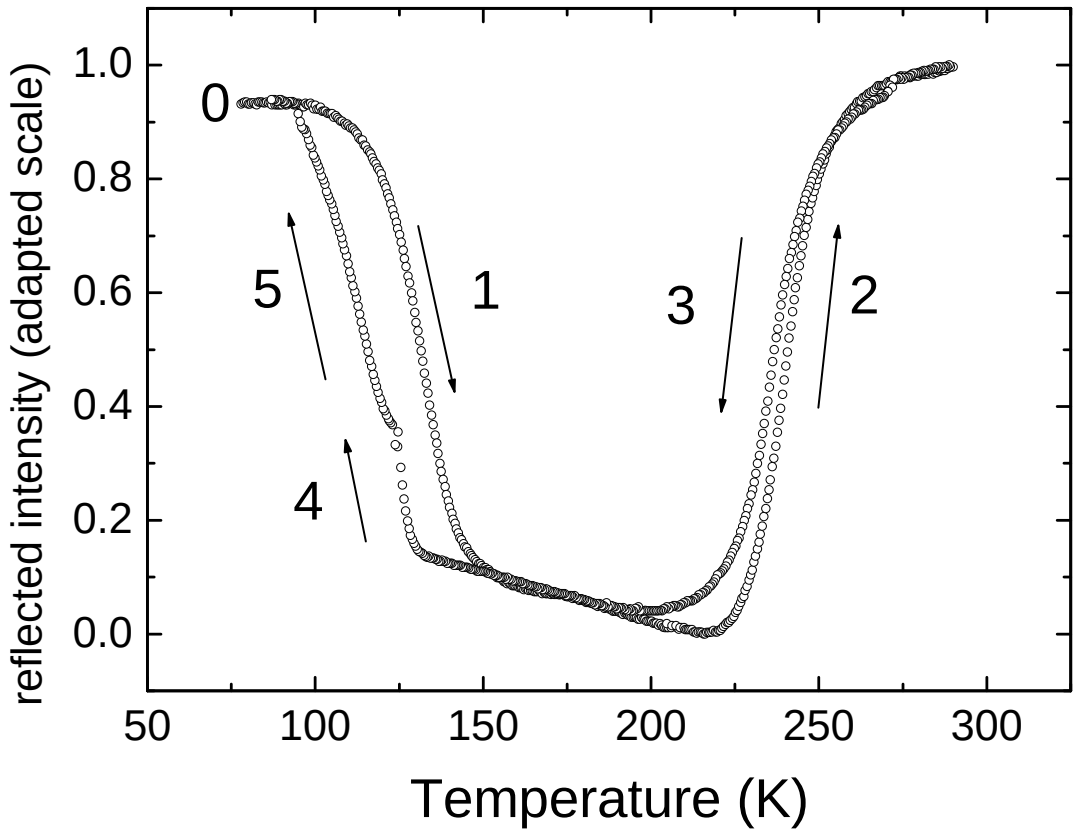

FIG. 10: Diffuse reflectance data under constant irradiation, obtained after photoexcitation overnight at 80K. Effective scan rates were 0.18, 0.25, 0.20, 0.004, and 0.18K/min for sections 1 to 5, respectively.

observed to be in the range $10 - 50$nm[42].

IV. DISCUSSION

A. Comparison to the Na-analogue (relaxation properties)

First we show the relaxation data of the Na-analogue, in Figure 14, with best-fitted curves using the same model as the one applied to the K-analogue. The agreement with the experimental data is excellent, even to long times. The fitting parameters are listed in Table IV. An Arrhenius plot leads to $E_a = 4600$ (70)K and $k_\infty = 1/\tau_0 \sim 1.0 \times 10^9 s^{-1}$ and a barrier energy of $E_{HL}(n_{HS} = 1/2) = E_a - \Delta \sim 3260$K in fair agreement with the value ~ 3420K reported by the previous analysis using a mean-field model based on a distribution of relaxation times[20].

Using these parameters we computed the transition curves for the Na-analogue shown in Figure 7, but failed to reproduce the 20K-wide experimental hysteresis. A possible explanation is based on the structural data reported in Ref. 10, which shows that the Q state undergoes an electronic relaxation towards a "Q-relaxed" state prior to the structural relaxation towards the LT state. The cooperativity associated with this latter transformation is missing during the electronic transformation observed by magnetic measurements. This explanation does not exclude the presence of distributions effects as assumed in Ref. 20, but they probably act to a lower extent since they are expected to be similar in the two analogous compounds.

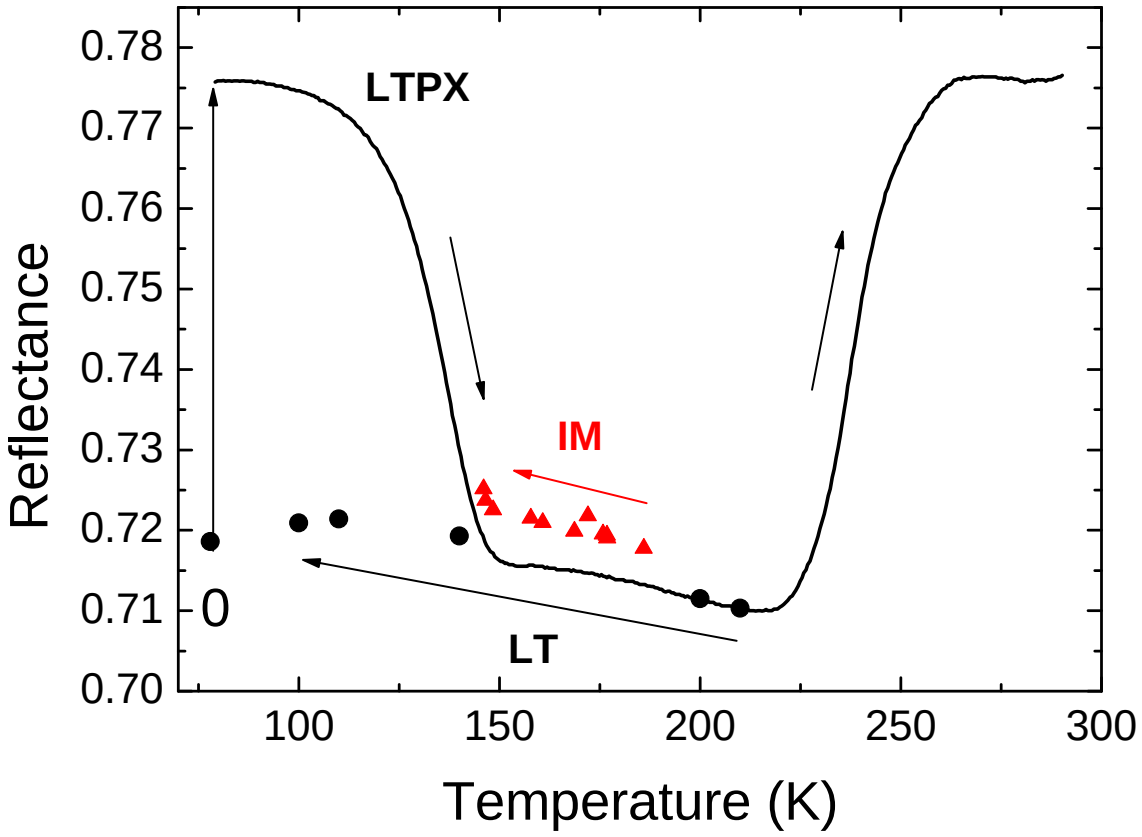

FIG. 11: Reflectance data obtained as snapshots under slow cooling from the HT state to generate the IM state (full triangles) or after relaxation of the PX state in the dark to generate the LT state (full circles). Both data sets are obtained on cooling. The data recorded under permanent light are shown for comparison (full line). Note that the snapshots around 200K after relaxation in the dark accurately match the full line.

State	T(K)	$1/\tau_0$ (s^{-1})	J (K)	J_{short} (K)	Scaling factor	HS residual
Q	130	0.262×10^{11}	11.8	78.0	0.995	0.006
	135	0.236×10^{11}	3.6	73.9	0.994	0.010
	140	0.209×10^{11}	2.3	86.7	0.991	0.010
	145	0.205×10^{11}	−10.7	86.1	0.991	0.013
	150	0.165×10^{11}	−26.2	77.9	0.993	0.012

TABLE IV: Refined parameter values for the isothermal relaxation curves of the Q-state of $Na_{0.32}Co[Fe(CN)_6]_{0.77} \cdot 4.4H_2O$ shown in Figure 14, using the correlation model with fixed value $E_a = 5000K$.

B. On the multi-step character of the thermal transition

The two-step character of the IMPX → LT relaxation, and of the HT → IM and LT → HT transformations of the K-compound was mentioned in the previous sections. A detailed inspection of the thermal transition in the Na-analog reveals a similar double-step character, Figure 15. It is worth noting that the shape of the thermal loop in the magnetic data of the Na-compound is reminiscent of the kinetic distortion due to the onset of the IM state in the K-compound. The multi-step character of the C_p anomaly at the LT → HT transformation of the K-compound, Figure 9, shows that this transformation is more complex than the simple succession of an electronic and a structural

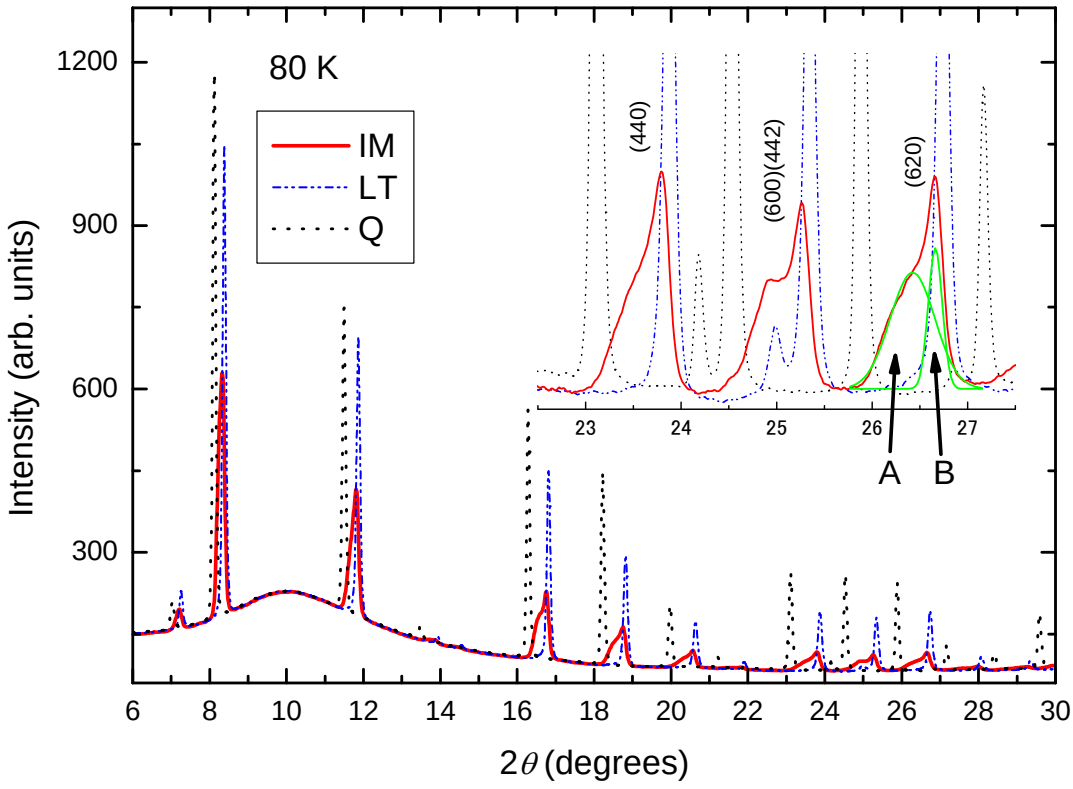

FIG. 12: X-ray diffraction pattern of the K-compound at 80K in the cooling branch of the IM state, with comparison to those of the LT and Q states. Inset: zoom of the most resolved lines, with analysis into Gaussian doublets (A=broad, B = narrow)

process.

C. The interaction parameter values

We turn now to a detailed inspection of the interaction parameters for the Q-state of the K- and Na-analogues (Tables II and IV). The two compounds exhibit similar values of the short-range parameter, but very different values of the long-range parameter, which is close to zero in the Na-analogue and mainly large and negative in the K-compound. In addition, the data for the K-compound exhibit large thermal dependences for both parameters, with some degree of correlation between them, while those of the Na-analogue remain almost temperature independent. We think that these different features result from the different natures of the processes. The complex behavior of the Q state of the K-compound should be associated with the twofold aspect of the process - electronic and structural - which in principle should involve two order parameters. It is conceivable that these two order parameters are governed by different activation energies and/or time scales and may result in a sizable temperature dependence of the "average parameters" presently used. Conversely, the approximate temperature independence of the fitted data for the Na-analogue suggests a relaxation process governed by a single order parameter that is electronic in nature. An alternative explanation might arise from the elastic nature of the interaction parameters, possibly leading to sizable thermal variations. Such is the case in the spin-Peierls transition[43,44], for example, in which the exchange interaction is modulated by the gradual dimerization of the lattice. Another important point is the opposite signs obtained for the short- and long-range interactions in the K- compound. It is well known that the presence of opposite interactions may lead to cluster formation, although whether or not this peculiarity is correlated to the creation of the IM state remains an open question.

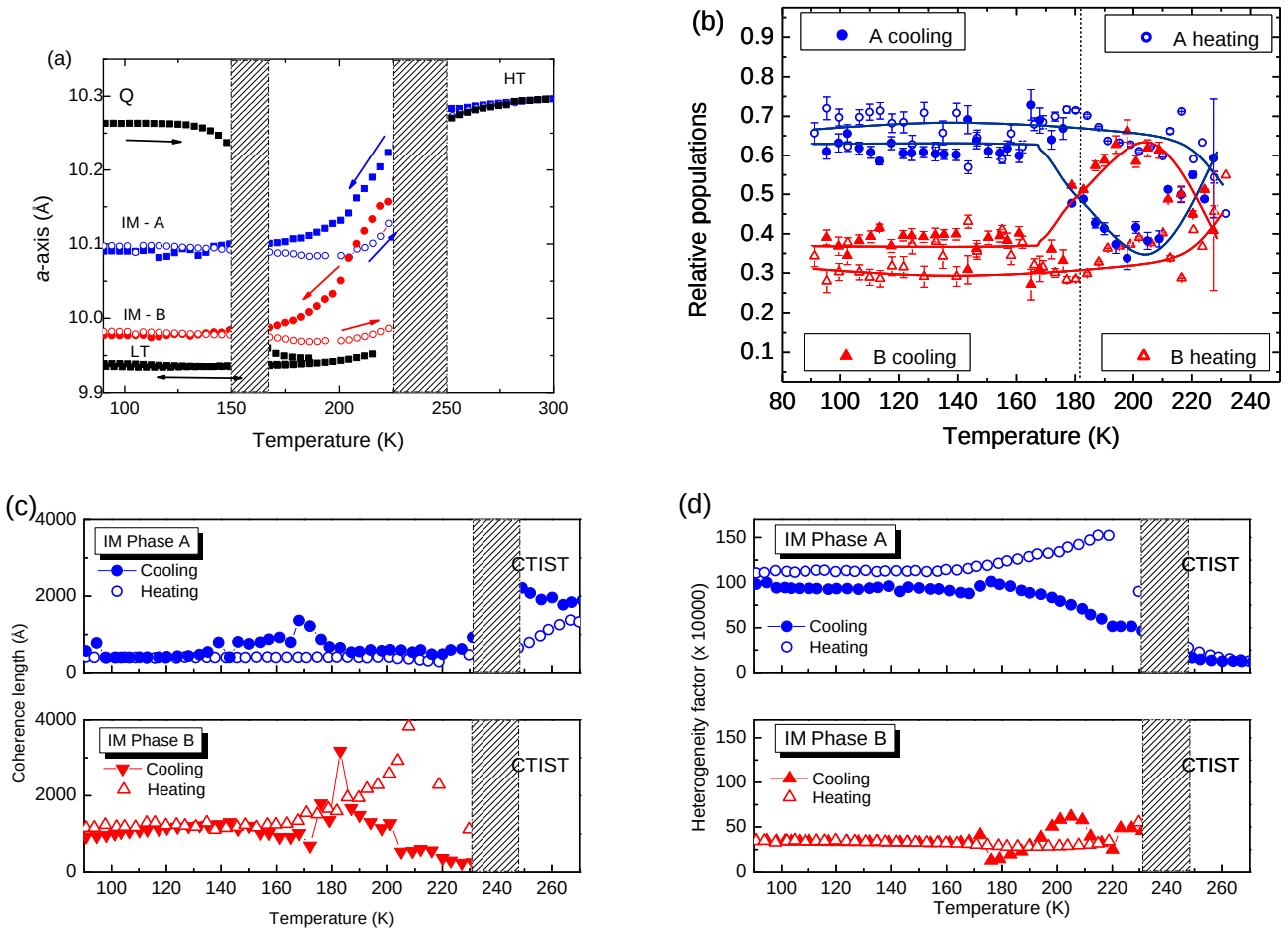

FIG. 13: Structural data of the IM phase during thermal cycling: (a) temperature dependence of the lattice parameter value in Q-, IM-A, IM-B, LT and HT phases; (b to d) temperature-dependence of the relative population (b), coherence length (c) and heterogeneity factor (d) of the IM-A (circles) and IM-B (triangles) states determined by application of the Stokes and Wilson formula. Solid/open symbols stands for cooling/heating runs.

D. On the possible origin of the IM state

We now discuss the physical properties of the IM state. The kinetic onset of the IM state and its short-range character imply a self-organization process. The driving force for this onset presumably originates from elastic stresses which are associated with the volume change upon the CTIST transformation. The short coherence length of the IM-A phase suggests the presence of strongly inhomogeneous stresses which compete against the cooperative character of the transition. These stresses finally result in a smooth transformation over a wide temperature range, yielding a slow relaxation regime upon cooling before the CTIST is completed. A similar effect of internal stresses upon a spin transition was recently illustrated in the spin-crossover compound $Fe(bbtr)_3(ClO_4)_2$ using optical microscopy. The inhomogeneous character of the transition in large crystals, due to the presence of internal stresses, resulted in large shifts (~ -20K) of the transition temperature in the stressed regions of the material[45,46]. Such a stress-based mechanism was able to explain the impact of the samples thermal history upon the spin transition temperature[47].

The self-organization process giving rise to the IM state certainly derives from elastic stresses resulting from the volume change associated with the CTIST process. We suggest that the growth of the IM state is a key factor affecting the stabilization of the quenched component, which would normally rapidly relax to the stable LT state, as it does in the Na-compound and other photo-magnetic Prussian Blue analogues. The onset of the microstructure presumably induces stresses which slow down the relaxation of the Q state. The coupling between the electronic and structural transformations involved in the CTIST process may also take part in this complex mechanism. Finally, as suggested by diffuse reflectance data, the self-organization process may be hindered by illumination, which is expected

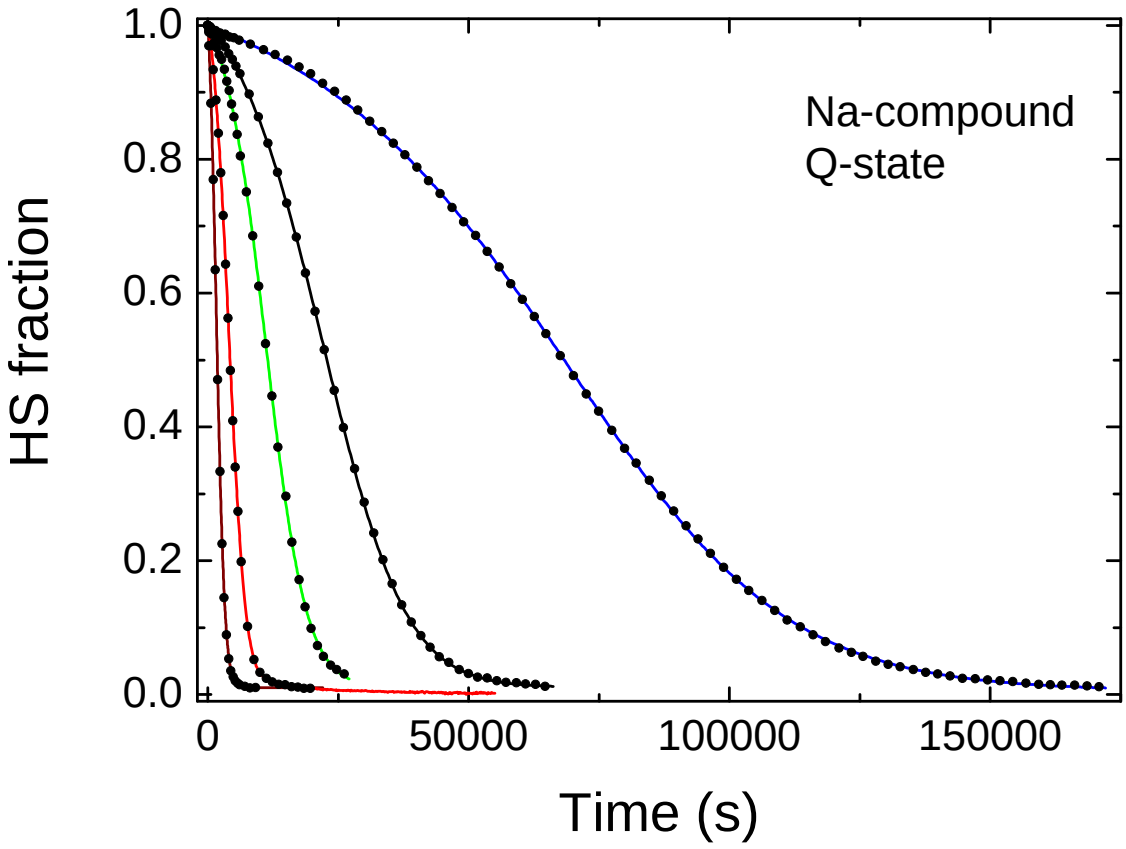

FIG. 14: Isothermal relaxation curves for the Q-state of $Na_{0.32}Co[Fe(CN)_6]_{0.74} \cdot 3.4H_2O$ at 150, 145, 140, 135 and 130K, left to right, adapted from Ref. 20 with best-fit computed curves using the present model. The fitting parameters are given in Table IV.

to randomize the distribution of HS and LS states in the lattice.

V. SUMMARY AND CONCLUSION

The unusual properties of the "intermediate" (IM) state obtained by slow cooling of the photo-magnetic Prussian Blue analogue $K_{0.3}Co[Fe(CN)_6]_{0.77} \cdot 4.4H_2O$have been described, while characterizing the magnetic properties of the different low-temperature states, including the quenched (Q), slow-cooled (IM) and low-temperature (LT) states, along with the corresponding photo-excited states, LTPX and IMPX. From the relaxation properties of the metastable Q, LTPX and IMPX states, it is inferred that the IM state is a mixture of the Q-type and LT phases. This conclusion is confirmed by X-ray diffraction. Further investigations show the fragile character of the IM state with respect to fatigue and irradiation by visible light. Calorimetric data support the complex character of the thermal transition, which was previously observed for the $Na_{0.32}Co[Fe(CN)_6]_{0.74} \cdot 3.4H_2O$ analogue. For both compounds the relaxation curves have been analyzed using a two-variable correlation model, which nicely predicts the experimental data. On the other hand, whereas the model reproduces the thermal hysteresis of the Na-compound, the agreement is less for the K-analogue, further illustrating the complex character of the transformations in the title compound. The origin of the IM state is attributed to a self-organization process, and a complete structural investigation of the system will be reported separately.

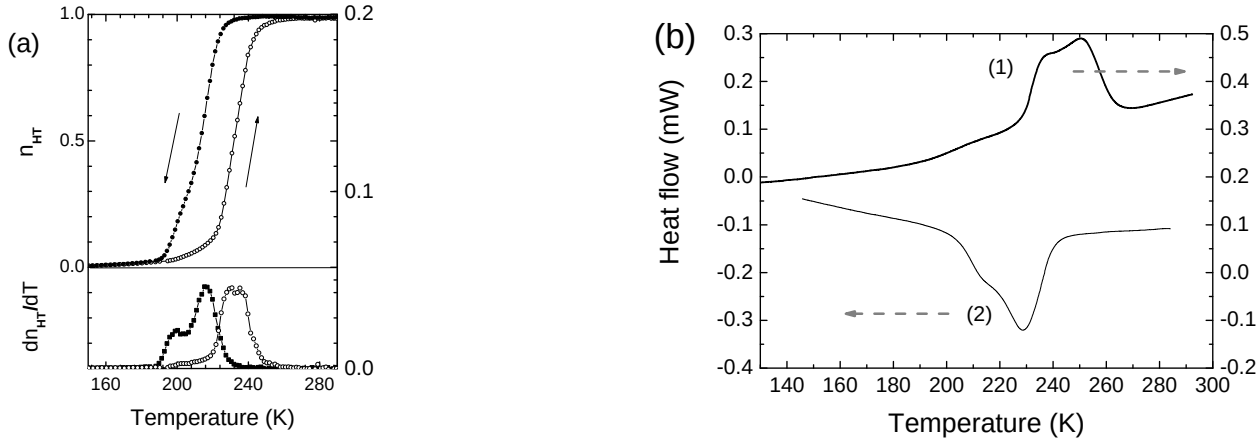

FIG. 15: Thermal transition hysteresis loop of $Na_{0.32}Co[Fe(CN)_6]_{0.74} \cdot 3.4H_2O$, from magnetic measurements (a) and from calorimetric measurements (b). Adapted from Refs. 20,21 respectively.

Acknowledgments

This work was supported by CNRS, Versailles and Bordeaux Universities, Région Ile-de-France et Région Aquitaine, projects MAT2007 − 61621 and CSD2007 − 00010 from the Spanish Ministerio de Educación y Ciencia and European Union Network of Excellence MAGMANet (contract: NMP3-CT−2005 − 515767 − 2) and partially supported by the US National Science Foundation through grants DMR???0453362 and DMR-1005581 (DRT). The authors thank Professor Mark W. Meisel for insights, and J. H. Park for early contributions to this work, and Matthew Andrus for verifying the chemical analysis.

* Present address : Dr. Miho Itoi
Division of Physics, Institute of Liberal Education, Nihon University School of Medecine,
Oyaguchi Kamicyo 30-1,
Itabashi 173-8010, Japan
† corresponding author : kbo@physique.uvsq.fr
‡ correponsding author : varret˙francois@yahoo.fr

[1] S. Ferlay, T. Mallah, R. Ouahs, P. Veillet, and M. Verdaguer, Nature **378**, 6558 (1995).
[2] O. Sato, T. Iyoda, A. Fujishima, and K. Hashimoto, Science **272**, 704 (1996).
[3] F. Varret, A. Goujon, J. Jeftic, M. Noguès, A. Bousseksou, S. Klokishner, A. Dolbecq, and M. Verdaguer, Hyperfine Interact. **113**, 37 (1998).
[4] F. Varret, M. Noguès, and A. Goujon, "Magnetism??: Molecules to materials," (J. Miller, M. Drillon, Wiley-VCH, 2001) Chap. 2, p. 257.
[5] P. Gütlich, Y. Garcia, and T. Woike, Coord. Chem. Rev. **219-221**, 839 (2001).
[6] M. Soraï, Chem. Soc. Jpn **74**, 2223 (2001).
[7] F. Varret, K. Boukheddaden, E. Codjovi, and A. Goujon, Hyperfine Interact. **165**, 37 (2005).
[8] T. Yokoyama, T. Ohta, O. Sato, and K. Hashimoto, Phys. Rev. B **58**, 8257 (1998).
[9] T. Yokoyama, M. Kiguchi, T. Ohta, O. Sato, Y. Einaga, and K. Hashimoto, Phys. Rev. B **60**, 9340 (1999).
[10] I. Maurin, D. Chernyshov, F. Varret, A. Bleuzen, H. Tokoro, K. Hashimoto, and S.-I. Ohkoshi, Phys. Rev. B **79**, 064420 (2009).
[11] T. Yamauchi, A. Nakamura, Y. Morimoto, T. Hozumi, K. Hashimoto, and S. Okhoshi, Phys. Rev. B **72**, 214425 (2005).
[12] Y. Moritomo, F. Nakada, H. Kamioka, T. Hozumi, and S. Ohkoshi, Phys. Rev. B **75**, 214110 (2007).
[13] V. Escax, A. Bleuzen, C. C. dit Moulin, F. Villain, A. Goujon, F. Varret, and M. Verdaguer, J. Am. Chem. Soc. **123**, 12536 (2001).
[14] J.-F. Letard, P. Guionneau, L. Rabardel, J. A. K. Howard, A. E. Goeta, D. Chasseau, and O. Kahn, Inorg. Chem. **37**, 4432 (1998).
[15] J. S. Costa, P. Guionneau, and J.-F. Létard, Second Int. Conf. on Photo-Induced Phase Transitions, J. of Physics: Conf. Series **21**, 67 (2005).
[16] O. Sato, Y. Einaga, T. Iyoda, A. Fujishima, and K. Hashimoto, Electrochem. Soc. **144**, L11 (1997).
[17] A. Goujon, O. Roubeau, M. Noguès, F. Varret, A. Dolbecq, and M. Verdaguer, Eur. Phys. J. B **14**, 115 (2000).
[18] A. Bleuzen, C. Lomenech, V. Escax, F. Villain, F. Varret, C. C. dit Moulin, and M. Verdaguer, J. Am. Chem. Soc. **122**, 6648 (2000).
[19] D. A. Pejakovic, J. L. Manson, J. S. Miller, and A. J. Epstein, Synthetic metals **122**, 529 (2001).
[20] S. Gawali, F. Varret, I. Maurin, C. Enachescu, M. Malarova, K. Boukheddaden, E. Codjovi, H. Tokoro, S. Ohkoshi, and K. Hashimoto, J. Phys. Chem. B **109**, 8251 (2005).
[21] M. Castro, J. Rodríguez-Velamazán, K. Boukheddaden, F. Varret, H. Tokoro, and S. Ohkoshi, Eur. Phys. Lett. **79**, 27007 (2007).
[22] J.-H. Park, F. Frye, N. E. Anderson, D. M. Pajerowski, Y. D. Huh, D. R. Talham, and M. W. Meisel, J. Magn. Magn. Mat. **310**, 1458 (2007).
[23] M. Itoi, in preparation .
[24] C. Enachescu, F. Varret, E. Codjovi, J. Linarès, S. Floquet, P. Manikandan, and P. Manoharan, J. Phys. Chem. B **110(12)**, 5883 (2006).
[25] C. J. O'Connor, Prog. Inorg. Chem. **29**, 203 (1982).
[26] W. Morscheidt, E. Codjovi, J. Jeftic, J. Linarès, A. Bousseksou, H. Constant-Machado, and F. Varret, Meas. Sci. Techn. **9**, 1311 (1998).
[27] A. Goujon, F. Varret, V. Escax, A. Bleuzen, and M. Verdaguer, Polyhedron **20**, 1347 (2001).
[28] F. Varret, A. Goujon, and A. Bleuzen, Hyperfine Interact. **134**, 69 (2001).
[29] V. Mishra, R. Mukherjee, J. Linares, C. Balde, C. Desplanches, J. Létard, E. Collet, L. Toupet, M. Castro, and F. Varret, Inorg. Chem. **47**, 7577 (2008).
[30] H. Mishra, V. Mishra, F. Varret, R. Mukherjee, C. Balde, C. Desplanches, , and J.-F. Létard, Polyhedron **28**, 1678 (2009).
[31] V. Mishra, H. Mishra, R. Mukherjee, E. Codjovi, J. Linarès, J.-F. Létard, C. Desplanches, C. Baldé, C. Enachescu, and F. Varret, Dalton Trans. , 7462 (2009).
[32] A. Bleuzen, J.-D. Cafun, A. Bachschmidt, M. Verdaguer, P. Munsch, F. Baudelet, and J.-P. Itie, J. Phys. Chem. C **112(45)**, 17709 (2008).
[33] L. H. Böttger, A. I. Chumakov, C. M. Grunert, P. Gütlich, J. Kusz, H. Paulsen, U. Ponkratz, V. Rusanov, A. X. Trauwein, and J. A. Wolny, Chem. Phys. Lett. **429(1-3)**, 189 (2006).
[34] A. Hauser, J. Alder, and P. Gütlich, Chem. Phys. Lett. **152**, 468 (1988).
[35] H. Romstedt, H. Spiering, and P. Gütlich, J. Phys. Chem. Solids **59**, 1353 (1998).
[36] B. Hôo, K. Boukheddaden, and F. Varret, Eur. Phys. J. B. **17**, 449 (2000).
[37] A. Hauser, J. Jeftic, H. Romstedt, R. Hinek, and H. Spiering, Coord. Chem. Rev. **190-192**, 471 (1999).
[38] A. Desaix, O. Roubeau, J. Jeftic, J. G. Haasnoot, K. Boukheddaden, E. Codjovi, J. Linares, M. Nogues, and F. Varret, Eur. Phys. J. B **6**, 183 (1998).

[39] F. Varret, K. Boukheddaden, J. Jeftic, and O. Roubeau, J. Mol. Cryst. Liq. Cryst. **335**, 1273 (1999).
[40] A. R. Stokes and A. J. C. Wilson, Proc. Camb. Phil. Soc. **38**, 313 (1942).
[41] A. R. Stokes and A. J. C. Wilson, Proc. Phys. Soc. (London) **56**, 174 (1944).
[42] M. Hanawa, Y. Morimoto, J. Tateishi, K. Kato, M. Takata, and M. Sakata, J. Phys. Soc. Jpn. **72**, 987 (2003).
[43] E. Pytte, Phys. Rev. B **10**, 4637 (1974).
[44] G. Beni, J. Chem. Phys. **58**, 3200 (1973).
[45] C. Chong, *Observation et modelisation d'effet d'auto-organisation dans les solides thermo et photo commutable*, Ph.D. thesis, Université de Versailles (April 2010).
[46] C. Chong, A. Slimani, F. Varret, K. Boukheddaden, E. Collet, J.-C. Ameline, R. Bronisz, and A. Hauser, Chem. Phys. Lett. **504**, 29 (2011).
[47] I. Krivokapic, C. Enachescu, R. Bronisz, and A. Hauser, Chem. Phys. Lett. **455**, 192 (2008).